Bean seedling growth enhancement using magnetite nanoparticles

Nádia M. Duran[a], Maria Medina-Llamas[b], João G. B. Cassanji[a], Rafael G. de Lima[a], Eduardo de Almeida[a], Willian R. Macedo[c], Davide Mattia[b] and Hudson W. Pereira de Carvalho[a,*]

[a]Laboratory of Nuclear Instrumentation (LIN), Center for Nuclear Energy in Agriculture (CENA), University of São Paulo (USP), Piracicaba, SP, 13416000, Brazil.

[b]Department of Chemical Engineering, University of Bath, BA2 7AY Bath, United Kingdom.

[c]Crop Physiology and Metabolism Lab, Institute of Agricultural Science, Federal University of Viçosa, Campus Rio Paranaíba, Rio Paranaíba, MG, 38810000, Brazil.

*Corresponding author:

Email: hudson@cena.usp.br

Phone: + 55 19 3429 4737

ABSTRACT

Advanced fertilizers are one of the top requirements to address rising global food demand. This study investigates the effect of bare and polyethylene glycol-coated Fe_3O_4 nanoparticles on the germination and seedling development of *Phaseolus vulgaris* L. Although the germination rate was not affected by the treatments (1 to 1 000 mg Fe L^{-1}), seed soaking in Fe_3O_4-PEG at 1 000 mg Fe L^{-1} increased radicle elongation (8.1 ± 1.1 cm vs. 5.9 ± 1.0 cm for the control). Conversely, $Fe^{2+}/Fe^{3+}_{(aq)}$ and bare Fe_3O_4 at 1 000 mg Fe L^{-1} prevented the growth. X-ray spectroscopy and tomography showed that Fe penetrated in the seed. Enzymatic assays showed that Fe_3O_4-PEG was least harmful treatment to α-amylase. The growth promoted by the Fe_3O_4-PEG might be related to water uptake enhancement induced by the PEG coating. These results show the potential of using coated iron nanoparticles to enhance the growth of common food crops.

KEYWORDS: *Phaseolus vulgaris* L., Fe_3O_4 nanoparticle, polyethylene glycol, germination, X-ray spectroscopy

INTRODUCTION

Due to the increase in human population, the agriculture is under pressure to intensify the use of chemical fertilizers to meet food demand. And yet, a large portion of fertilizers directly applied to the soil is lost by water leaching, irreversible/strong adsorption or, in the case of nitrogen sources, by evaporation. This loss negatively affects the environment, the sustainability of the sources of mineral inputs and the economic performance of agricultural activity. In this context, using nano-sized fertilizers could significantly increase uptake by plants, paving the way to a more sustainable strategy to improve nutrient delivery.[1]

Although Fe is the second most abundant metal in the earth's crust,[2] it is mostly found as Fe^{3+} oxides and oxyhydroxides in cultivated (aerated) soils, which are insoluble (goethite, ferrihydrite and hematite with K_{sp} values ranging from 10^{-37} to 10^{-44}).[3] This means that even though the total Fe content is high, its availability to plants is still low. Iron uptake can be divided in two categories: Strategy I for nongraminaceous plants and Strategy II for graminaceous. Nongraminaceous species take up Fe by three reactions: (i) excreting protons from the roots to the rhizosphere, reducing the soil solution pH and thus increasing Fe^{3+} solubility; (ii) reducing Fe^{3+} to Fe^{2+} by Fe^{3+}-chelate reductase; (iii) plasmalemma transport of Fe^{2+} by iron transporters. Roots of graminaceous species release phytosiderophores that chelate Fe^{3+} in the rhizosphere, and then specific plasmalemma transporters take the Fe^{3+}-phytosiderophores complexes.[4]

In plants, Fe plays an important role in the photosynthetic activity, biosynthesis of many enzymes, Fe-S protein clusters and heme proteins like cytochromes, is required for chloroplast thylakoids structure and maintenance, and chlorophyll synthesis.[2]

Iron oxide nanoparticles are currently used in a wide range of applications, as drug delivery systems contrast agents in magnetic resonance imaging and for hyperthermia treatments; in the production of magnetic inks or magnetic seals in motors, to name a few.[5] In the agricultural

scenario, the effects of iron nanoparticles have been observed in the uptake, transport, accumulation and development of plant species. It was previously demonstrated that these nanoparticles accumulate in pumpkin plants tissues,[6] stimulate the development of peanut[7] and watermelon[8] seedlings, but did not affect growth and chlorophyll content of lettuce.[9] In all instances, iron nanoparticle effects vary according to their chemical composition, size, morphology, aggregation state, applied concentration as well as experimental conditions like temperature and time of exposure.

Magnetite nanoparticles are prone to aggregation due to a combined effect of their high surface area to volume ratio and their strong magnetization, thus limiting their use for bio-applications.[10] To address the former problem, magnetite nanoparticles are usually synthesised in the presence of surfactants, which form a coating layer preventing aggregation. Common surfactants are polyethylene glycol (PEG), polyvinyl alcohol (PVA), Polyvinylpyrrolidone (PVP), poly lactic-co-glycolic acid (PLGA), chitosan and dextran.[11] Among them, PEG is a hydrophilic polymer widely used for biomedical applications, being biocompatible, non-immunogenic, and non-antigenic.[12]

In this work, we report the effect of Fe_3O_4-PEG and bare Fe_3O_4 nanoparticles on the germination and seedling development of *Phaseolus vulgaris* L. (common bean) seeds. The effects of 1, 10, 100 and 1 000 mg Fe L^{-1} seed soaking treatments was observed on the germination rate, radicle elongation and α-amylase activity of 5-days old seedlings. X-ray fluorescence spectroscopy (XRF) and X-ray tomography uncovered the Fe uptake and spatial distribution.

MATERIALS AND METHODS

Synthesis of Iron Oxide Nanoparticles. Bare magnetite nanoparticles (nFe_3O_4) were synthetized by a co-precipitation method using a mixture of iron (III) chloride tetrahydrate

(FeCl$_2$·4H$_2$O) and iron (II) chloride hexahydrate (FeCl$_3$·6H$_2$O), both purchased from Sigma-Aldrich, at a 2:1 molar ratio of Fe^{3+}:Fe^{2+}, m_{FeCl3} = 7.00 g, m_{FeCl2} = 2.58 g in 300 ml DI water. The solution was poured in a three-neck round bottom flask provided with a condenser, nitrogen and liquid inlets. Then 0.5 ml of a 37 % wt. HCl were added under gentle agitation. Oxygen was purged using nitrogen for 20 minutes prior the addition of 100 ml 1.5 M NH$_4$OH. The solution quickly turned black, indicating the beginning of the production of the nanoparticles. The reaction lasted 1 h at 20 ˚C and nitrogen was supplied during the whole reaction. After the synthesis, the nanoparticles were washed using cycles of deoxygenated DI water and magnetic decantation. Then, the nanoparticles were dried at room temperature under vacuum for 24 h and immediately characterized.

A slightly modified procedure was used to produce Fe$_3$O$_4$-PEG nanoparticles (nFe$_3$O$_4$-PEG), which consisted in dissolving the iron salts in 300 ml of a 10 % wt PEG (M_w 10 000) in DI water solution prior the addition of NH$_4$OH. Reaction and washing conditions were the same as described above.

Characterization of Pristine Fe$_3$O$_4$ Nanoparticles and Dispersions. The composition of each set of nanoparticles was determined by energy dispersive X-ray fluorescence spectroscopy (EDXRF; EDX-720 Shimadzu, Japan). The quantification was carried out using the fundamental parameters method (see the Supporting Information). Crystal size and phase identification were determined by X-ray diffraction (XRD), using a Bruker D8-Advance diffractometer (Bruker-AXS GmbH, Karlsruhe, Germany) with Cu Kα radiation. Measurements were recorded for 2θ values from 20 to 80˚. Nanoparticle size and morphology were evaluated via transmission electron microscopy (TEM; JEOL, JEM-2100 Plus, USA). The coated and uncoated magnetite nanoparticles were suspended in deionized water and dispersed using an ultrasonic processor (model 705 Sonic Dismembrator, Fisher Scientific, USA) under 50% amplitude for 15 min, with 30 s interval every minute, at 1, 10, 100 and 1 000 mg Fe L^{-1}.

The hydrodynamic size and the zeta potential of the nanomaterials at 100 mg Fe L^{-1} were analyzed via dynamic light scattering (DLS; Zetasizer Nano, Malvern Instruments, UK).

Germination Assay. The effects of nFe_3O_4 and nFe_3O_4-PEG on the germination of *Phaseolus vulgaris* L. seeds were evaluated. Since one-third of the Fe atoms in magnetite occurs as Fe^{2+} and two-thirds occurs as Fe^{3+},[13] an iron ionic reference treatment (herein referred as soluble-Fe) was prepared as a mixture of one-third of $FeSO_4.7H_2O$ and two-thirds of $Fe_2(SO_4)_3.nH_2O$, both purchased from Reagen (Brazil).

Phaseolus vulgaris L. seeds, cultivar Sintonia, were supplied by the Agronomic Institute of Campinas (IAC), presented an average germination rate of 80%. This seed was chosen as model species because it has low dormancy, it results in a plant of small size and short growth cycle, making it an ideal test case. In addition, *P. vulgaris* is an important and accessible source of protein.[14]

Seeds were first immersed in a 10% NaClO solution under stirring for 10 s for disinfection, followed by rinsing with deionized water. Subsequently, twenty seeds were soaked for 20 min in the appropriate concentration of nFe_3O_4 and nFe_3O_4-PEG dispersions. Soluble-Fe solutions at the same concentrations were used as a positive control, whereas deionized water was used as a negative control. After exposure, the seeds were placed on a 15-cm paper filter fit on the bottom of a Petri dish, and 8 mL of the soaking solution was added to moisturize the paper filter. The Petri dishes were sealed with Parafilm M (Bemis Company Inc., USA), inserted into a plastic bag to prevent water loss, and finally incubated in a germination chamber (TE-4020, Tecnal, BR) under dark and ventilation at 27 °C for five days. The experiment was conducted in five replicates per treatment.

After five days of the sowing, the assay was completed and the number of germinated seeds was counted to determine the rate of germination. The radicle length of the seedlings was measured, manually removed and weighted. After that, both radicles and seeds were rinsed with

deionized water to remove the surface-bound metal or nano metal oxide and then dried in a laboratory oven (515/4A, FANEM, Brazil) at 60 °C for two days.

Radicle Length Determination. At the end of the germination period, the five replicates of seedlings from each treatment were separately transferred to a black cardboard, then a HP Scanjet 2410 scanner operated by Photosmart software was used to obtain scanned images of the seedlings. The radicle length (cm) of the seedlings was determined through the digitized images using the Seed Vigor Imaging System software (SVIS®).[15]

Iron Uptake Quantification. Replicates from each treatment were grouped and the dried seedlings were carefully separated in three fractions: cotyledon, seed coat and radicle. The cotyledons were then ground using a mortar mill (MA890, Marconi, Brazil). One gram of each component was weighed in a decontaminated porcelain crucible and then digested by dry ashing method using a muffle furnace (F-2, Fornitec, Brazil) at 100 °C h^{-1} ramp rate up to 550°C and then ashed for 14 h. Each dry ashing digestion batch included a blank to ensure no contamination. The ashes were dissolved in 5 mL of 1 M $HNO_{3(aq)}$, then 200 µL of this solution plus 750 µL of ultrapure water was transferred into a 1.5 mL vial, and 50 µL of 1 000 mg Ga L^{-1} was added as an internal standard. Then, the sample was homogenized using a tube shaker vortex (MA162, Marconi, Brazil).

The Fe content of the digested samples was determined by EDXRF. For that, 10 µL of the digests were pipetted on the external side of the window of a 6.3 mm XRF sample cup (no. 3577 - Spex Ind. Inc., USA) and sealed with a 5 µm thick polypropylene film (no. 3520 - Spex Ind. Inc., USA). The cups were then left dry in a laboratory oven at 60°C. The samples were analyzed in triplicate using a rhodium (Rh) X-ray tube at 50 kV and auto-tunable current with a deadtime at 30% and a 3-mm collimator. The X-ray spectrum of the sample was acquired utilizing a Si (Li) detector for 200 s. The quantification was performed using external standard calibration. The trueness of this method was assessed analyzing two certified reference

materials: apple leaves (NIST 1515) and peach leaves (NIST 1547).

Mapping Fe Accumulation Spots. The seeds were exposed to nFe_3O_4, nFe_3O_4-PEG and soluble-Fe at 1 000 mg Fe L^{-1} for 20 min, dried at room temperature and gently cut in the middle using a stainless steel blade. Subsequently, the seeds were placed on a sample holder with a Kapton tape and the cotyledon's inner side exposed for analysis.

The microanalysis was carried out using a benchtop microprobe X-ray fluorescence spectrometer (μ-XRF) system (Orbis PC EDAX, USA) operated with a Rh X-ray tube at 40 kV and 300 μA, and using a 25 μm Ni filter. A polycapillary optic provided a 30 μm X-ray beam spot size. The detection was carried out by a 30 mm^2 silicon drift detector (140 eV FWHM at the 5.9 keV Mn-Kα line) with a deadtime of nearly 3%. Maps were registered using a matrix of 64x50 pixels (number of analyzed points on xy- axes) and dwell time per pixel of 1 s. The experimental setup is illustrated in Figure S1 of the Supporting Information.

3D Distribution of Fe in the Hilum. Common beans have a hilum associated to the seed coat, and near the hilum there is the micropyle, a small pore that allows water uptake into the seed.[16] We employed X-ray tomography to verify the 3D distribution of Fe in the hilum region of treated seeds.

Common bean seeds were exposed to nFe_3O_4-PEG and soluble-Fe at 1 000 mg Fe L^{-1} for 20 min and dried at room temperature. A small fraction of the seed coat containing the hilum were carefully collected and cut using a razor blade.

Tomograms were acquired at the X-ray imaging beamline (IMX) at the 1.37 GeV Brazilian Synchrotron Light Laboratory (LNLS, Campinas, Brazil). At IMX beamline, synchrotron radiation was generated by a bending-magnet. The measurements were carried out using a pink beam from 4 to 14 keV and 1024 projections were taken under 180° rotation. The exposure time was 300 ms per projection. The image was magnified and focused on a cooled camera detector (CCD; PCO.2000, PCO, Germany). Pictures of the sample holders containing the seed coat

fractions and the experimental X-ray tomography setup are presented in Figures S2 and S3, respectively, of the Supporting Information.

To complement this data, these samples were also submitted to μ-XRF mapping. The analysis parameters and experimental setup were the same as above mentioned (mapping Fe accumulation spots).

Reactivity of Soluble-Fe and Magnetite Nanoparticles. The reactivity of the soluble-Fe and magnetite nanoparticles was evaluated measuring their ability to decompose H_2O_2[17] through a Fenton-like reaction.[18] In a 25 mL round-bottom reaction flask, 19.5 mL of a 1 000 mg Fe L^{-1} aqueous dispersion of the tested nanoparticles and soluble-Fe solution was magnetically stirred. The flask was connected to a 25 mL graduated pipette through a silicone tube. The pipette was immersed in a measuring cylinder water column. Then, 0.5 mL of 30% v/v H_2O_2 solution was inserted in the reaction flask with a syringe. The volume of the produced O_2 was monitored by following the shift of a water column in pipette (see experimental setup at Figure S4 of the Supporting Information).

α-amylase Activity. The evaluations for the α-amylase enzyme followed the recommendations of Fuwa.[19] *P. vulgaris* seeds were soaked in nFe_3O_4, nFe_3O_4-PEG and soluble-Fe at 1 000 mg Fe L^{-1} for 20 min and then germinated in paper rolls inside a germination chamber (Mangelsdorf, DeLeo, Brazil) at 25°C. The experiment was conducted in quadruplicate, with 20 seeds per replicate. The seedlings were collected on the 7th day after sowing, subsequently nearly 1 g were weighed and macerated using a mortar and pestle in a phosphate buffer solution (pH 6.9) at a 9:1 (distilled water: buffer) ratio. This material was centrifuged for 4 min at 12 000 g (NT 805, Novatecnica, Brazil), then the supernatant was removed for the enzymatic analysis, and 1% starch solution was used as the substrate. The value of 1 U (Enzymatic Unit) was considered to be the reduction of 10% of the colorimetric intensity of the amylose-iodine complex.

Statistical Analysis. The number of germinated seeds and the radicle length and weight data were submitted to analysis of variance (ANOVA) and Tukey's multiple range tests at 95% confidence interval using the Action Stat software (version 3.3.111.1178, Estatcamp, BR).

RESULTS AND DISCUSSION

Characterization of the Nanoparticles and Dispersions. The purity of the nFe_3O_4 and Fe_3O_4-PEG was determined by EDXRF. Considering the limits of detection of the method, in the order of mg kg^{-1}, no contaminants were found in the nanoparticles. Figure S5 in the Supporting Information presents the XRF spectra for these samples. XRD patterns, presented in Figure S6, showed that the average crystallite size in the direction of the plane (220) were 11.6 and 13.9 nm for the uncoated and coated magnetite nanoparticles, respectively (see the crystallite size in the direction of the other planes in Table S1 of the Supporting Information). These results were in good agreement with the observations by transmission electron microscopy (TEM) (Figure S7), which presumed an average particle size of 11 nm for nFe_3O_4 and 12 nm for Fe_3O_4-PEG.

The DLS measurements (Table 1) revealed that in aqueous dispersions the nanoparticles used for seed priming formed aggregates (DLS curves are in Figure S8). The values are in broad agreement with reported values of 208 ± 15 nm for 50-60 nm nFe_3O_4 suspended in water at 10 mg L^{-1} and 438 ± 13 nm at 20 mg L^{-1}.[9] One could visually observe that such aggregates make these magnetite dispersions very unstable. At 1 000 mg Fe L^{-1}, most was settled after 60 min, and even in the nFe_3O_4-PEG case. Zeta-potential measurements indicated that the uncoated magnetite presented a negative value, while the PEG coated had a positive result. The pH registered for the uncoated magnetite dispersion used in these analyses was 5.58 and 5.08 for the PEG coated dispersion. A possible explanation to the former behavior is the steric hindrance over the surface active sites produced by the adsorption of polymers with high molecular

weight, such as PEG.[20] The measured ζ-potential for the uncoated samples was different from values reported in the literature, 4.31 ± 0.05 mV for the less concentrated dispersion (10 mg L^{-1}) and 3.99 ± 0.4 mV for the highest one (20 mg L^{-1}).[9]

Effects of Magnetite Nanoparticles on *P. vulgaris* Seed Germination and Radicle Growth. The number of germinated seeds was daily counted and all the radicles emerged almost in the same period. At the end of the germination assay, the deionized water treatment control gave an average germination rate of 88.8% (Figure 1). All the others treatments had higher or comparable values to the negative control. The highest germination rate was found for 1 mg Fe L^{-1} of nFe_3O_4 and 10 mg Fe L^{-1} of nFe_3O_4-PEG (97 and 96%, respectively). However, under ANOVA statistical analysis, no difference was found among treatments and controls ($p < 0.05$).

Although the treatments did not affect the germination rate, a different scenario was observed in the radicle elongation of the seedlings. The phenotypic images of the seedlings after 5 days of Fe treatments exposure (Figure 2) indicate that the highest applied concentration was toxic for the seedlings development, but this was not observed for the nFe_3O_4-PEG treatment.

The average length of the radicle of negative control was 5.9 ± 1.0 cm long, whilst nFe_3O_4 and soluble-Fe at 1 000 mg Fe L^{-1} shortened it yielding 2.9 ± 0.5 and 1.2 ± 0.3 cm, respectively. Conversely, PEG improved the radicle development even at its higher concentration, where the highest radicle elongation of 8.1 ± 1.1 cm was observed (Figure 3a). This effect can be attributed to the hydrophilic nature of the PEG,[21] which may have aided in root growth by redirecting water to a region close to the root of the seedlings, an effect caused by the reduction of water potential, thus determining greater water absorption by the tissue and consequently its growth. In addition, the distribution of nanoparticles on seed coat were more homogeneous

241 when PEG was added. This led to a controlled absorption of nFe_3O_4, by the reduction of the
242 water surface tension.[22]

243 After the length measurements, the radicles were removed and weighed (Figure 3b). The same
244 trend was observed for length and weight, radicles from water treatment presented 1.94 ± 0.13
245 g and nFe_3O_4 at 1 000 mg Fe L^{-1} had 0.82 ± 0.09 g. According to the Tukey's test ($p < 0.05$),
246 radicle length was significantly different from the control at 1 000 mg Fe L^{-1} for all the tested
247 materials, positively for nFe_3O_4-PEG and negatively for nFe_3O_4 and soluble-Fe treatments
248 (Figure S9). However, radicle weight data was only statistically different from control for
249 nFe_3O_4 and soluble-Fe at 1 000 mg Fe L^{-1} (Figure S10).

250 The phytotoxicity observed for high concentrations of soluble-Fe and nFe_3O_4 might be related
251 to the accumulation of this element in the seed tissues. Such statement is reinforced by fact that
252 the absorption of soluble-Fe occurs mainly by the micropyle, the determinant structure for water
253 imbibition by seeds,[23] mainly in the initial stages of the germination process, as will be
254 discussed in depth bellow.

255 Studies reported root shortening as the concentration of nanoparticle in the dispersion
256 increases. This was demonstrated for ZnO,[24, 25] Ag,[26] CuO[27, 28] and TiO_2.[29] The anomalous
257 behavior found for Fe in the present study was also observed for white mustard, where the root
258 elongation of the seedlings treated with the highest nFe_3O_4 concentrations (100 and 1 000 mg
259 L^{-1}) was higher than the lower tested concentration (10 mg L^{-1}), although the difference was
260 not statistically significant.[30] On the other hand, soybean and rice seeds treated with γ-Fe_2O_3
261 nanoparticles at 500, 1 000 and 2 000 mg L^{-1} developed seedlings with the root elongation
262 significantly higher than the control.[31, 32]

263 Nano zerovalent iron at 5 000 mg L^{-1} also promoted the root elongation of *Arabidopsis*
264 *thaliana* by 150-200% compared to the control, with the elongation caused by hydroxyl radical-
265 induced cell wall loosening.[33] Other authors observed that γ-Fe_2O_3 nanoparticles promoted the

growth of peanut by regulating the antioxidant enzyme activity and the content of abscisic acid, a phytohormone that stimulates the senescence and reduces the metabolism. The peanut root dry biomass was increased by Fe_2O_3 nanoparticles at 1 000 mg kg^{-1} applied to the soil.[34]

Since PEG is hydrophilic, it can prevent the nFe_3O_4-PEG from interacting with cells and/or proteins.[12] In animal cells, the surface chemistry modification of iron oxide nanoparticles by PEG reduced the cytotoxicity and the formation of reactive oxygen species (ROS), with the cell length not affected compared to those treated with bare nanoparticles.[35] The uptake of PEG-coated magnetite by macrophage cells was much lower than that of uncoated nanoparticles.[36, 37]

Determination of Fe uptake by *P. vulgaris* seeds. After the germination assays, the seedling tissues were divided and the Fe content was determined. These tissues are presented in the Figure S11 of the Supporting Information. Figure 4 presents the concentration of Fe in the (a) seed coat, (b) cotyledon and (c) radicle of the seedlings exposed to nFe_3O_4, nFe_3O_4-PEG, soluble-Fe and water negative control.

The negative control (deionized water) revealed that Fe is more concentrated in the seed coat of the tested common beans than in the others tissues analyzed. It presented 92.3 ± 0.6 mg Fe kg^{-1}, in contrast to 46.6 ± 1.4 mg Fe kg^{-1} in the cotyledons and 72.8 ± 0.5 mg Fe kg^{-1} in the radicle. In the case of the seedlings that received nanoparticle treatment, those that were soaked in nFe_3O_4 presented similar Fe content in the three analyzed regions, regardless of the applied concentration. The difference between the water control and nFe_3O_4 treatment reached a maximum value of 50% in the seed coat sample that was soaked in 1 000 mg Fe L^{-1}, while this difference was more than 6 000-fold higher for the soluble-Fe treatment. At the highest treatment concentration, the incorporation of Fe from the nFe_3O_4-PEG in the seed coat and in the radicle was intermediate between those of nFe_3O_4 and soluble-Fe.

Intending to estimate the contribution of dissolved Fe on the seedling development and Fe uptake, solubility tests in deionized water were performed as described in the Supporting Information. For nFe_3O_4 and nFe_3O_4-PEG dispersions at 100 and 1 000 mg Fe L^{-1}, the soluble Fe fractions were not quantitatively detected, i.e. they were below the limit of quantification of the method (0.15 mg Fe L^{-1}). In a study carried out by Landa et al.[30] it was found 6.51 ± 2.24 mg Fe L^{-1} in the supernatant of a cultivation medium supplemented with nFe_3O_4 at 1 000 mg L^{-1}. However, it is important to keep in mind that the presence of other molecules can induce the generation of soluble complexes with Fe.

Due to the low solubility, one can hypothesize that Fe was mainly taken up by the seedling tissues as intact magnetite nanoparticles. These nanoparticles then could undergo dissolution within the plant tissues. The chemical speciation of the incorporated Fe will be addressed in further studies.

Spatial Distribution of Fe in the Primed Seeds. Figure 5 presents the internal side of the cotyledon of a *P. vulgaris* seeds soaked for 20 min in (a) nFe_3O_4-PEG and (b) soluble-Fe at 1 000 mg Fe L^{-1}. The results corroborate the quantitative analysis, indicating that the treatments concentrated Fe in the seed coat, mainly in the hilum region, and the number of XRF counts was almost 5-fold higher for the soluble-Fe treatment compared to the nanoparticle one.

Additional μ-XRF chemical maps were recorded specifically in the hilum region of the treated seeds. The images of the Fe distribution in the hilum revealed a different pattern of distribution between seeds soaked in nFe_3O_4-PEG dispersion and soluble-Fe solution at 1 000 mg Fe L^{-1} (Figure 6). The nanoparticle treatment concentrated Fe mainly in the edge around the hilum (Figure 6a), while soluble-Fe presented a hotspot in the micropyle (Figure 6b). Other study[38] using magnetic resonance microscopy showed that during the imbibition process, water enters the *P. vulgaris* seed through the micropyle, and consequently, this is the channel for soluble Fe ions.

315 The hilum is a sponge-like tissue (see Figure S12 in the SI), thus besides sticking on the
316 tissue's outer surface, the nanoparticles can penetrate through the channels reaching internal
317 layers. In spite of X-ray fluorescence's high analytical sensitivity, it yielded only 2D maps. The
318 6.4 keV Kα photons emitted by Fe atoms embedded in the seed coat can escape from a depth
319 that lies in the mm range. As such, the images shown in Figure 6 cannot tell whether Fe is only
320 adsorbed on the surface of the seed coat or whether it was also inside the hilum tissue.
321 Hence, the hilum region of treated seeds was subjected to further X-ray tomography analysis.
322 Figure 7 shows 3D projections and slices of phase contrast tomography for the seed coat of
323 seeds soaked in (a) nFe_3O_4-PEG and (b) soluble-Fe at 1 000 mg Fe L^{-1} for 20 min. The greenish
324 regions, highlighted by the red circles, indicate the presence of Fe that penetrated within the
325 hilum sponge tissue. This can be observed for both nFe_3O_4-PEG and soluble-Fe. The
326 combination of μ-XRF and X-ray tomography unequivocally showed that Fe supplied in
327 nanoparticulate form could enter in the seeds.
328 X-ray tomography was previously employed to understand physiological seed development
329 of rice,[39] maize[40] and oilseed rape,[41] observe germination behavior of sugar beet seeds,[42] and
330 also to analyze archaeological seeds in the investigation of crop domestication.[43, 44] However,
331 to the best of our knowledge, no other study examined 3D images of a nanoparticle-treated bean
332 seed, although some researchers used this technique to verify the uptake and distribution of
333 gold and yttrium nanoparticles in *Arabidopsis thaliana*[45] and cabbage plants.[46]
334 **Chemical Reactivity of nFe_3O_4 and nFe_3O_4-PEG.** The chemical reactivity of the tested
335 materials was accessed through the volume of O_2 produced during the degradation of H_2O_2 by
336 the magnetite nanoparticles and soluble-Fe used for seed soaking. The most reactive
337 nanoparticle was nFe_3O_4 which produced 12.4 mL of O_2 in 300 min, while nFe_3O_4-PEG
338 produced 7.5 mL in the same time. On the other hand, soluble-Fe readily produced 22.1 mL in
339 8 min (Figure S13). Iron catalyzes the decomposition of H_2O_2 trough Fenton reaction. The high

reactivity of the soluble-Fe is due to the availability of free ionic Fe that leads to homogenous Fenton reaction, which is faster than the heterogeneous one.[47] On the other hand, the lower reactivity of the PEG coated nanoparticles may be the result of a lower number of available Fe sites, since the nanoparticle surface is sterically hindered by the polymeric chains. This result may explain the non-deleterious effects caused by the coated nanoparticles in the radicle elongation, even at high concentrations.

α-amylase Activity. The energy source necessary for the germination and early seedling development of leguminous comes mainly from the degradation of proteins and carbohydrates present in the seed reserves. Protein and starch comprise about 20% and 40% of the whole *P. vulgaris* seed, respectively.[48] Here we evaluated the α-amylase (starch degrading enzyme) activity in the seedlings whose seeds were soaked in nFe_3O_4, nFe_3O_4-PEG and soluble-Fe at 1 000 mg Fe L^{-1}.

Compared to the result that was obtained for the non-treated seeds (1600 ± 300 U), soluble-Fe treatment presented the lowest enzymatic activity, followed by nFe_3O_4 (730 ± 30 and 760 ± 140 U, respectively). Reinforcing what was observed in the radicle development and in the chemical reactivity analysis, nFe_3O_4-PEG treatment was the least harmful to the α-amylase activity (900 ± 180 U) (Table S2).

α-amylase is a metalloenzyme which needs Ca^{2+} to its activity and stability, its affinity is much stronger than that with others ions.[49] Since Fe^{2+} is also a divalent ion, its presence in abundance could provoke a competition with Ca^{2+} during the α-amylase biosynthesis, leading to enzymatic activity loss. This possibility is supported by the previously observed reduction of amylase activity *in vitro* in fish intestine after Fe^{2+} addition (50 mg kg^{-1}).[50]

Figure S14 attempts to correlate the radicle length and weight to the content of Fe incorporated by the seedling tissues. Although the Fe amount in the seedling tissues was very similar, the biologic effects were distinct: The deleterious effects caused by 1 000 mg Fe L^{-1}

soluble-Fe can be attributed to phytotoxicity due the excess of this element, as previously discussed. However, the growth promotion induced by nFe_3O_4-PEG cannot be explained solely by the content of Fe incorporated by the seedlings. Since the highest seedling growth and weight gain were observed for the nFe_3O_4-PEG, and this treatment did not yield the highest α-amylase activity, one can infer that the decomposition of starch was not the limiting factor for the seedling development.

We previously demonstrated that Cu from CuO nanoparticles were mostly concentrated in the seed coat of *P. vulgaris* seeds after soaking, especially in the hilum region,[28] but now thanks to X-ray microtomography we concluded that Fe from magnetite nanoparticles was not only absorbed on the surface of the seed coat, but also penetrated the hilum tissue, an evidence that nanoparticles can enter in the seeds.

Although the root elongation and shortening caused by nanoparticles seed treatment were already demonstrated for cucumber treated with ZnO[25] and CuO,[51] corn soaked in ZnO,[25] mung bean exposed to Ag,[26] and even for white mustard treated with magnetite nanoparticle,[30] nothing was reported so far about the influence of coated nanoparticle on the root length. Even though the mechanisms involved in this phenomenon is not well understood, the literature states that nanoparticles can penetrate root cells membranes, enhance water uptake and consequently induce the root elongation.[52]

The presented paper also highlighted that the PEG coating turn the nanoparticles less reactive than uncoated one. It was already demonstrated that surfactant coated nanoparticles can be less toxic than their uncoated counterparts.[53, 54] Besides the PEG coating, the radicle growth can be also related to an intermediated content of Fe uptake by the radicles. As above mentioned, the radicle elongation for other plant species also increased as the applied Fe nanoparticle concentration raised.[30-32]

Altogether, the results showed that nanomaterials are potential candidates for seed priming.

390 The deleterious effects of magnetite nanoparticles were smaller than those shown by aqueous
391 Fe^{3+}/Fe^{2+}. Thus, the supplying of nutrients through sources of intermediate solubility makes
392 phytotoxicity less prone to occur. Rather than only transferring nutrients to the roots, X-ray
393 fluorescence and tomography showed that the nanoparticles can penetrate within the seed
394 structure and thus modify the seedling development. Finally, the PEG coating played a major
395 role on the properties of the magnetite nanoparticles and might be responsible for the growth
396 promotion reported in this study.
397

ABBREVIATIONS USED

Fe_3O_4	magnetite
PEG	polyethylene glycol
PVA	polyvinyl alcohol
PVP	polyvinylpyrrolidone
PLGA	poly lactic-co-glycolic acid
XRF	X-ray fluorescence spectroscopy
nFe_3O_4	magnetite nanoparticles
nFe_3O_4-PEG	magnetite nanoparticles covered with polyethylene glycol
$FeSO_4.7H_2O$	iron(II) sulfate heptahydrate
$Fe_2(SO_4)_3.nH_2O$	iron(III) sulfate hydrate
EDXRF	energy dispersive X-ray fluorescence spectroscopy
XRD	X-ray diffraction
TEM	transmission electron microscopy
DLS	dynamic light scattering
LNBio	Brazilian Biosciences National Laboratory
IAC	Agronomic Institute of Campinas
NaClO	sodium hypochlorite
SVIS ®	Seed Vigor Imaging System
LPV	Department of Crop Science
ESALQ	"Luiz de Queiroz" College of Agriculture
USP	University of São Paulo
ANOVA	analysis of variance
HNO_3	nitric acid
μ-XRF	micro probe X-ray fluorescence spectroscopy

423	IMX	X-ray imaging beamline
424	LNLS	Brazilian Synchrotron Light Laboratory
425	CCD	cooled camera detector
426	H_2O	water
427	H_2O_2	hydrogen peroxide
428	U	Enzymatic Unit
429	ZnO	zinc oxide
430	CuO	copper(II) oxide
431	TiO_2	titanium dioxide
432	Fe_2O_3	maghemite
433	ROS	reactive oxygen species

434

435 **ACKNOWLEDGMENT**

436 The authors are grateful for Prof. Silvio Moure Cícero and Dr. Francisco Guilhien Gomes
437 Junior from "Luiz de Queiroz" College of Agriculture, University of São Paulo
438 (LPV/ESALQ/USP), for the support and to provide the Image Analysis Laboratory facilities.
439 We thank LNLS for beamtime at IMX beamline (proposal 2016-06626) and Prof. Eduardo F.
440 Molina (UNIFRAN) for assistance during beamtime. Dr. Alisson Chiorato from IAC is also
441 acknowledged for supplying the e the *Phaseolus vulgaris* seeds, cultivar Sintonia.

442

443 **FUNDING**

444 This study was supported by FAPESP Young Investigators Award 2015/05942-0, FAPESP
445 SPRINT 2016-50014-6 and FAPESP Multiuser Equipment Program 2015/19121-8. CAPES
446 (Coordination for the Improvement of Higher Education Personnel) is acknowledged for
447 granted scholarship to N.M.D.

SUPPORTING INFORMATION

The Supporting Information is available free of charge on the ACS Publications website at DOI: Purity and contaminant analysis of nFe_3O_4 and Fe_3O_4-PEG (EDXRF methodology and spectra); XRD analysis methodology, diffractograms and crystallite size of the magnetite nanoparticles; µ-XRF experimental setup; X-ray tomography imaging experimental setup; Experimental setup and results for the nFe_3O_4 and Fe_3O_4-PEG reactivity analysis; TEM images of nFe_3O_4 and Fe_3O_4-PEG; DLS curves; Statistical analysis (Tukey test); Pictures of the three fractions of the seedlings (seed coat, cotyledon and radicle) analyzed by EDXRF; methodology and quantitative results of the solubility tests carried out with the nFe_3O_4 and Fe_3O_4-PEG dispersions; SEM image of the hilum of a *P. vulgaris* seed; α-amylase activity in the germinated treated beans; Correlation between radicle length and weight with the content of Fe incorporated by the seedling tissues (seed coat, cotyledon and radicle).

REFERENCES

(1) Raliya, R.; Saharan, V.; Dimkpa, C.; Biswas, P. Nanofertilizer for precision and sustainable agriculture: current state and future perspectives. *J. Agric. Food Chem.* **2017**, DOI: 10.1021/acs.jafc.7b02178.

(2) Marschner, P. *Mineral Nutrition of Higher Plants*. 3rd. ed.; Academic Press: San Diego, 2012; 672 pages.

(3) Schwertmann, U. Solubility and dissolution of iron-oxides. *Plant Soil* **1991,** *130*, 1-25.

(4) Romheld, V.; Marschner, H. Evidence for a specific uptake system for iron phytosiderophores in roots of grasses. *Plant Physiol.* **1986**, *80*, 175-180.

(5) Figuerola, A.; Di Corato, R.; Manna, L.; Pellegrino, T. From iron oxide nanoparticles towards advanced iron-based inorganic materials designed for biomedical applications. *Pharmacol. Res.* **2010,** *62*, 126-143.

(6) Zhu, H.; Han, J.; Xiao, J. Q.; Jin, Y. Uptake, translocation, and accumulation of manufactured iron oxide nanoparticles by pumpkin plants. *J. Environ. Monitor.* **2008,** *10*, 713-717.

(7) Li, X.; Yang, Y. C.; Gao, B.; Zhang, M. Stimulation of peanut seedling development and growth by zero-valent iron nanoparticles at low concentrations. *Plos One* **2015,** *10*, 12.

(8) Li, J. L.; Chang, P. R.; Huang, J.; Wang, Y. Q.; Yuan, H.; Ren, H. X. Physiological effects of magnetic iron oxide nanoparticles towards watermelon. *J. Nanosci. Nanotechno.* **2013,** *13*, 5561-5567.

(9) Trujillo-Reyes, J.; Majumdar, S.; Botez, C. E.; Peralta-Videa, J. R.; Gardea-Torresdey, J. L. Exposure studies of core-shell Fe/Fe_3O_4 and Cu/CuO NPs to lettuce (*Lactuca sativa*) plants: Are they a potential physiological and nutritional hazard? *J. Hazard. Mater.* **2014,** *267*, 255-263.

(10) Gupta, A. K.; Gupta, M. Synthesis and surface engineering of iron oxide nanoparticles for biomedical applications. *Biomaterials* **2005,** *26*, 3995-4021.

(11) Laurent, S.; Forge, D.; Port, M.; Roch, A.; Robic, C.; Elst, L. V.; Muller, R. N. Magnetic iron oxide nanoparticles: Synthesis, stabilization, vectorization, physicochemical characterizations, and biological applications. *Chem. Rev.* **2008,** *108*, 2064-2110.

(12) Gupta, A. K.; Wells, S. Surface-modified superparamagnetic nanoparticles for drug delivery: preparation, characterization, and cytotoxicity studies. *IEEE Trans. NanoBiosci.* **2004,** *3*, 66-73.

(13) Yamashita, T.; Hayes, P. Analysis of XPS spectra of Fe^{2+} and Fe^{3+} ions in oxide materials. *Appl. Surf. Sci.* **2008,** *254*, 2441-2449.

(14) Rossi, G. B.; Valentim-Neto, P. A.; Blank, M.; de Faria, J. C.; Arisi, A. C. M. Comparison of grain proteome profiles of four brazilian common bean (*Phaseolus vulgaris* L.) cultivars. *J. Agric. Food Chem.* **2017,** *65*, 7588-7597.

(15) Sako, Y.; McDonald, M. B.; Fujimura, K.; Evans, A. F.; Bennett, M. A. A system for automated seed vigour assessment. *Seed Sci. Technol.* **2001**, *29*, 625-636.

(16) Vieira, C.; Paula Júnior, T. J.; Borém, A. Botânica. In *Feijão*. 2 ed.; Universidade Federal de Viçosa: Viçosa, Brazil, 2006; 600 pp.

(17) Silva, A. C.; Oliveira, D. Q. L.; Oliveira, L. C. A.; Anastacio, A. S.; Ramalho, T. C.; Lopes, J. H.; Carvalho, H. W. P.; Torres, C. E. R. Nb-containing hematites $Fe_{2-x}Nb_xO_3$: The role of Nb^{5+} on the reactivity in presence of the H_2O_2 or ultraviolet light. *Appl. Catal. a-Gen.* **2009,** *357*, 79-84.

(18) Carvalho, H. W. P.; Hammer, P.; Pulcinelli, S. H.; Santilli, C. V.; Molina, E. F. Improvement of the photocatalytic activity of magnetite by Mn-incorporation. *Mater. Sci. Eng. B-Solid.* **2014,** *181*, 64-69.

(19) Fuwa, H. A new method for microdetermination of amylase activity by the use of amylose as the substrate. *J. Biochem.* **1954,** *41*, 583-603.

(20) Liufu, S.; Xiao, H.; Li, Y. Investigation of PEG adsorption on the surface of zinc oxide nanoparticles. *Powder Technol.* **2004,** *145*, 20-24.

(21) Thijs, H. M. L.; Becer, C. R.; Guerrero-Sanchez, C.; Fournier, D.; Hoogenboom, R.; Schubert, U. S. Water uptake of hydrophilic polymers determined by a thermal gravimetric analyzer with a controlled humidity chamber. *J. Mater. Chem.* **2007,** *17*, 4864-4871.

(22) Schwuger, M. Mechanism of interaction between ionic surfactants and polyglycol ethers in water. *J. Colloid Interf. Sci.* **1973,** *43*, 491-498.

(23) Das, B.; Saha, P. K. Ultrastuctural dimorphism of micropyle determines differential germinability of *Sesbania cannabina* seeds. *Seed Sci. Technol.* **2006,** *34*, 363-372.

(24) Lin, D. H.; Xing, B. S. Phytotoxicity of nanoparticles: Inhibition of seed germination and root growth. *Environ. Pollut.* **2007,** *150*, 243-250.

(25) Zhang, R. C.; Zhang, H. B.; Tu, C.; Hu, X. F.; Li, L. Z.; Luo, Y. M.; Christie, P. Phytotoxicity of ZnO nanoparticles and the released Zn(II) ion to corn (*Zea mays* L.) and cucumber (*Cucumis sativus* L.) during germination. *Environ. Sci. Pollut. R.* **2015,** *22*, 11109-11117.

(26) Nair, P. M. G.; Chung, I. M. Physiological and molecular level studies on the toxicity of silver nanoparticles in germinating seedlings of mung bean (*Vigna radiata* L.). *Acta Physiol. Plant.* **2015,** *37*, 11.

(27) Adams, J.; Wright, M.; Wagner, H.; Valiente, J.; Britt, D.; Anderson, A. Cu from dissolution of CuO nanoparticles signals changes in root morphology. *Plant Physiol. Bioch.* **2017,** *110*, 108-117.

(28) Duran, N. M.; Savassa, S. M.; de Lima, R. G.; de Almeida, E.; Linhares, F. S.; van Gestel, C. A. M.; de Carvalho, H. W. P. X-ray spectroscopy uncovering the effects of Cu based nanoparticle concentration and structure on *Phaseolus vulgaris* germination and seedling development. *J. Agric. Food Chem.* **2017,** *65*, 7874-7884.

(29) Castiglione, M. R.; Giorgetti, L.; Geri, C.; Cremonini, R. The effects of nano-TiO_2 on seed germination, development and mitosis of root tip cells of *Vicia narbonensis* L. and *Zea mays* L. *J. Nanopart. Res.* **2011,** *13*, 2443-2449.

(30) Landa, P.; Cyrusova, T.; Jerabkova, J.; Drabek, O.; Vanek, T.; Podlipna, R. Effect of metal oxides on plant germination: phytotoxicity of nanoparticles, bulk materials, and metal ions. *Water Air Soil Poll.* **2016,** *227*, 10.

(31) Alidoust, D.; Isoda, A. Effect of gamma Fe_2O_3 nanoparticles on photosynthetic characteristic of soybean (*Glycine max* (L.) Merr.): foliar spray versus soil amendment. *Acta Physiol. Plant.* **2013,** *35*, 3365-3375.

(32) Alidoust, D.; Isoda, A. Phytotoxicity assessment of gamma-Fe_2O_3 nanoparticles on root elongation and growth of rice plant. *Environ. Earth Sci.* **2014,** *71*, 5173-5182.

(33) Kim, J. H.; Lee, Y.; Kim, E. J.; Gu, S.; Sohn, E. J.; Seo, Y. S.; An, H. J.; Chang, Y. S. Exposure of iron nanoparticles to *Arabidopsis thaliana* enhances root elongation by triggering cell wall loosening. *Environ. Sci. Technol.* **2014,** *48*, 3477-3485.

(34) Rui, M. M.; Ma, C. X.; Hao, Y.; Guo, J.; Rui, Y. K.; Tang, X. L.; Zhao, Q.; Fan, X.; Zhang, Z. T.; Hou, T. Q.; Zhu, S. Y. Iron oxide nanoparticles as a potential iron fertilizer for peanut (*Arachis hypogaea*). *Front. Plant Sci.* **2016,** *7*, 10.

(35) Yu, M.; Huang, S. H.; Yu, K. J.; Clyne, A. M. Dextran and polymer polyethylene glycol (PEG) coating reduce both 5 and 30 nm iron oxide nanoparticle cytotoxicity in 2D and 3D cell culture. *Int. J. Mol. Sci.* **2012,** *13*, 5554-5570.

(36) Zhang, Y.; Kohler, N.; Zhang, M. Q. Surface modification of superparamagnetic magnetite nanoparticles and their intracellular uptake. *Biomaterials* **2002,** *23*, 1553-1561.

(37) Xie, J.; Xu, C.; Kohler, N.; Hou, Y.; Sun, S. Controlled PEGylation of monodisperse Fe_3O_4 nanoparticles for reduced non-specific uptake by macrophage cells. *Adv. Mater.* **2007,** *19*, 3163-3166.

(38) Mikac, U.; Sepe, A.; Sersa, I. MR microscopy for noninvasive detection of water distribution during soaking and cooking in the common bean. *Magn. Reson. Imag.* **2015,** *33*, 336-345.

(39) Jhala, V. M.; Thaker, V. S. X-ray computed tomography to study rice (*Oryza sativa* L.) panicle development. *J. Exp. Bot.* **2015,** *66*, 6819-6825.

(40) Rousseau, D.; Widiez, T.; Di Tommaso, S.; Rositi, H.; Adrien, J.; Maire, E.; Langer, M.; Olivier, C.; Peyrin, F.; Rogowsky, P. Fast virtual histology using X-ray in-line phase tomography: application to the 3D anatomy of maize developing seeds. *Plant Methods* **2015,** *11*, 10.

(41) Verboven, P.; Herremans, E.; Borisjuk, L.; Helfen, L.; Ho, Q. T.; Tschiersch, H.; Fuchs, J.; Nicolai, B. M.; Rolletschek, H. Void space inside the developing seed of *Brassica napus* and the modelling of its function. *New Phytol.* **2013,** *199*, 936-947.

(42) Blunk, S.; Malik, A. H.; de Heer, M. I.; Ekblad, T.; Fredlund, K.; Mooney, S. J.; Sturrock, C. J. Quantification of differences in germination behaviour of pelleted and coated sugar beet seeds using x-ray computed tomography (x-ray CT). *Biomed. Phys. Eng. Express* **2017,** *3*, 11.

(43) Zong, Y. B.; Yao, S. K.; Crawford, G. W.; Fang, H.; Lang, J. F.; Fan, J. D.; Sun, Z. B.; Liu, Y.; Zhang, J. H.; Duan, X. L.; Zhou, G. Z.; Xiao, T. Q.; Luan, F. S.; Wang, Q.; Chen, X. X.; Jiang, H. D. Selection for oil content during soybean domestication revealed by X-ray tomography of ancient beans. *Sci. Rep-UK* **2017,** *7*, 10.

(44) Murphy, C.; Fuller, D. Q. Seed coat thinning during horsegram (*Macrotyloma uniflorum*) domestication documented through synchrotron tomography of archaeological seeds. *Sci. Rep-UK* **2017,** *7*, 9.

(45) Avellan, A.; Schwab, F.; Masion, A.; Chaurand, P.; Borschneck, D.; Vidal, V.; Rose, J.; Santaella, C.; Levard, C. Nanoparticle uptake in plants: gold nanomaterial localized in roots of *Arabidopsis thaliana* by X-ray computed nanotomography and hyperspectral imaging. *Environ. Sci. Technol.* **2017,** *51*, 8682-8691.

(46) Chen, Y. Y.; Sanchez, C.; Yue, Y.; de Almeida, M.; Gonzalez, J. M.; Parkinson, D. Y.; Liang, H. Observation of yttrium oxide nanoparticles in cabbage (*Brassica oleracea*) through dual energy K-edge subtraction imaging. *J. Nanobiotechnol.* **2016,** *14*, 10.

(47) Xavier, S.; Gandhimathi, R.; Nidheesh, P. V.; Ramesh, S. T. Comparison of homogeneous and heterogeneous Fenton processes for the removal of reactive dye Magenta MB from aqueous solution. *Desalin. Water Treat.* **2015,** *53*, 109-118.

(48) Marquezi, M.; Gervin, V. M.; Watanabe, L. B.; Bassinello, P. Z.; Amante, E. R. Physical and chemical properties of starch and flour from different common bean (*Phaseolus vulgaris* L.) cultivars. *Braz. J. Food Technol.* **2016**, 19, e2016005.

(49) Gupta, R.; Gigras, P.; Mohapatra, H.; Goswami, V. K.; Chauhan, B. Microbial alpha-amylases: a biotechnological perspective. *Process Biochem.* **2003,** *38*, 1599-1616.

(50) Li, J. S.; Li, J. L.; Wu, T. T. The effects of copper, iron and zinc on digestive enzyme activity in the hybrid tilapia *Oreochromis niloticus* (L.) x *Oreochromis aureus* (Steindachner). *J. Fish Biol.* **2007,** *71*, 1788-1798.

(51) Moon, Y. S.; Park, E. S.; Kim, T. O.; Lee, H. S.; Lee, S. E. SELDI-TOF MS-based discovery of a biomarker in *Cucumis sativus* seeds exposed to CuO nanoparticles. *Environ. Toxicol. Phar.* **2014,** *38*, 922-931.

(52) Wang, X. P.; Han, H. Y.; Liu, X. Q.; Gu, X. X.; Chen, K.; Lu, D. L. Multi-walled carbon nanotubes can enhance root elongation of wheat (*Triticum aestivum*) plants. *J. Nanopart. Res.* **2012,** *14*, 10.

(53) Nguyen, K. C.; Seligy, V. L.; Massarsky, A.; Moon, T. W.; Rippstein, P.; Tan, J.; Tayabali, A. F. Iop In *Comparison of toxicity of uncoated and coated silver nanoparticles*, 3rd International Conference on Safe Production and Use of Nanomaterials (Nanosafe), Minatec, Grenoble, FRANCE, Nov 13-15; Iop Publishing Ltd: Minatec, Grenoble, France, 2012.

(54) Suresh, A. K.; Pelletier, D. A.; Wang, W.; Moon, J. W.; Gu, B. H.; Mortensen, N. P.; Allison, D. P.; Joy, D. C.; Phelps, T. J.; Doktycz, M. J. Silver Nanocrystallites: Biofabrication using *Shewanella oneidensis*, and an evaluation of their comparative toxicity on gram-negative and gram-positive bacteria. *Environ. Sci. Technol.* **2010,** *44*, 5210-5215.

FIGURE CAPTIONS

Figure 1. Germination rate of *P. vulgaris* seeds exposed to nFe_3O_4, nFe_3O_4-PEG, soluble-Fe (1, 10, 100 and 1 000 mg Fe L^{-1}) and H_2O after 5 days of germination.

Figure 2. Seedlings of *P. vulgaris* whose seeds were soaked in (a) H_2O, (b) nFe_3O_4, (c) nFe_3O_4-PEG and (d) soluble-Fe. Applied concentrations were 1, 10, 100 and 1 000 mg Fe L^{-1}.

Figure 3. (a) Radicle length and (b) weight of *P. vulgaris* seedlings whose seeds were soaked in nFe_3O_4, nFe_3O_4-PEG, soluble-Fe (1, 10, 100 and 1 000 mg Fe L^{-1}) and H_2O (control).

Figure 4. Iron concentration in the (a) seed coat, (b) cotyledon and (c) radicle of germinated *P. vulgaris* seeds soaked in nFe_3O_4, nFe_3O_4-PEG and soluble-Fe at 1 000 mg Fe L^{-1} and H_2O.

Figure 5. μ-XRF chemical maps for Fe in *P. vulgaris* seeds soaked in (a) nFe_3O_4-PEG and (b) soluble-Fe at 1 000 mg Fe L^{-1}.

Figure 6. Pictures of the hilum of *P. vulgaris* seeds soaked in (a) nFe_3O_4-PEG and (b) soluble-Fe at 1 000 mg Fe L^{-1} and its corresponding μ-XRF chemical maps for Fe.

Figure 7. X-ray tomograms of the hilum of a *P. vulgaris* seed treated with (a) Fe_3O_4-PEG nanoparticle and (b) soluble-Fe at 1 000 mg Fe L^{-1} dispersion for 20 min. The greenish spots highlighted by the red circles indicates the presence of Fe embedded in the organic tissue.

TABLES

Table 1. Zeta potential and hydrodynamic diameter of nFe_3O_4 and nFe_3O_4-PEG dispersions determined by Dynamic Light Scattering (DLS).

Magnetite type	**Zeta-potential (mV)**	**Hydrodynamic Diameter (nm)**		
		Peak 1	*Peak 2*	*Peak 3*
nFe_3O_4	-14 ± 7	71 ± 10 (12%)	310 ± 60 (88%)	--
nFe_3O_4-PEG	9 ± 6	170 ± 60 (54%)	480 ± 150 (41%)	2 700 ± 160 (5%)

FIGURES

Figure 1

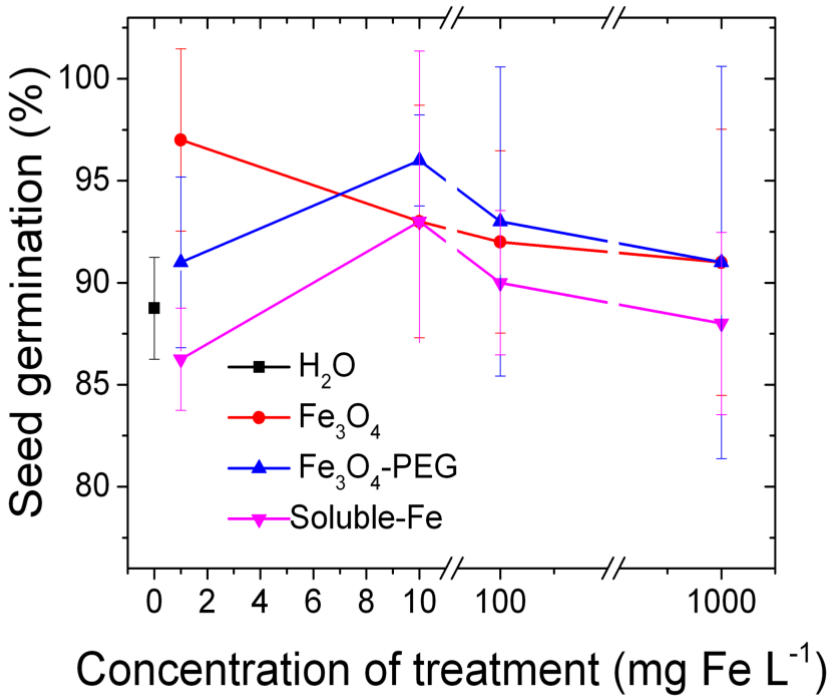

Figure 2

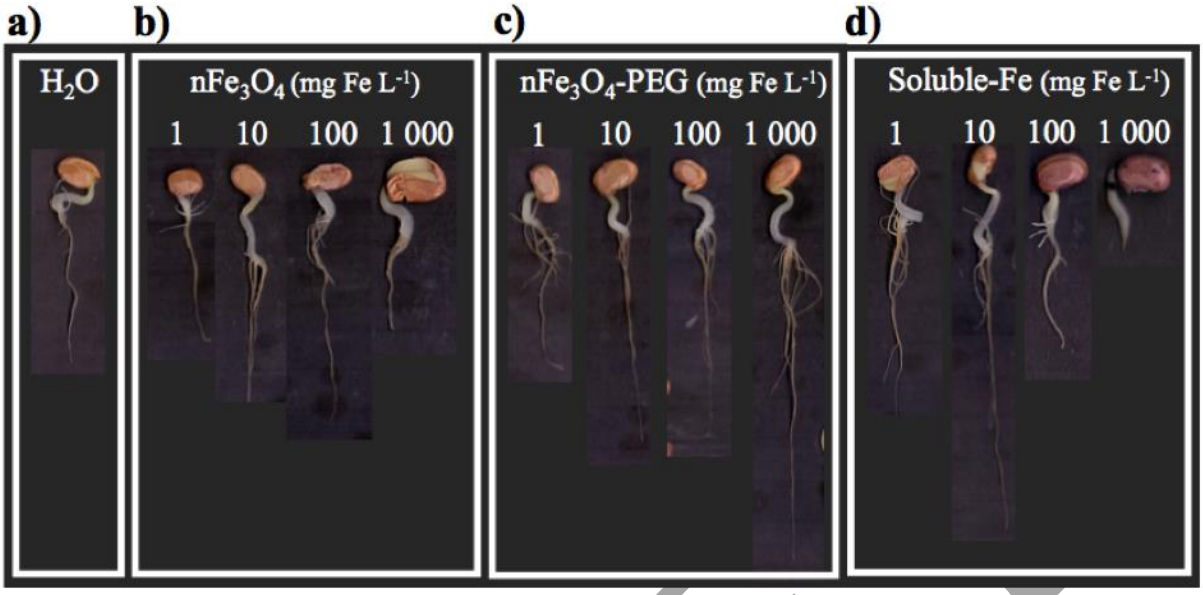

Figure 3

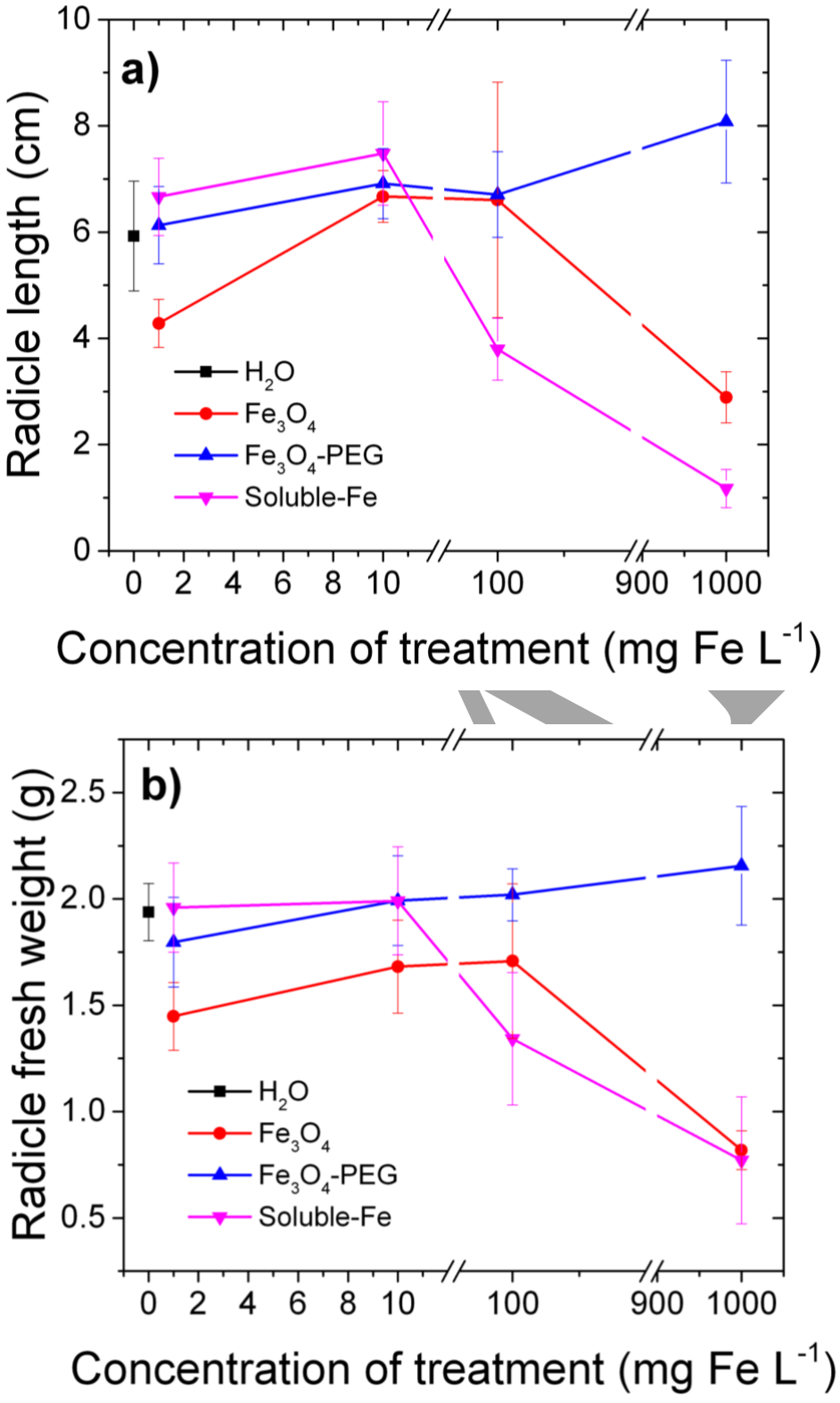
a)
Radicle length (cm)
0
2
4
6
8
10
0
2
4
6
8
10
100
900
1000
H2O
Fe3O4
Fe3O4-PEG
Soluble-Fe
Concentration of treatment (mg Fe L-1)
b)
Radicle fresh weight (g)
0.5
1.0
1.5
2.0
2.5
0
2
4
6
8
10
100
900
1000
H2O
Fe3O4
Fe3O4-PEG
Soluble-Fe
Concentration of treatment (mg Fe L-1)

Figure 4

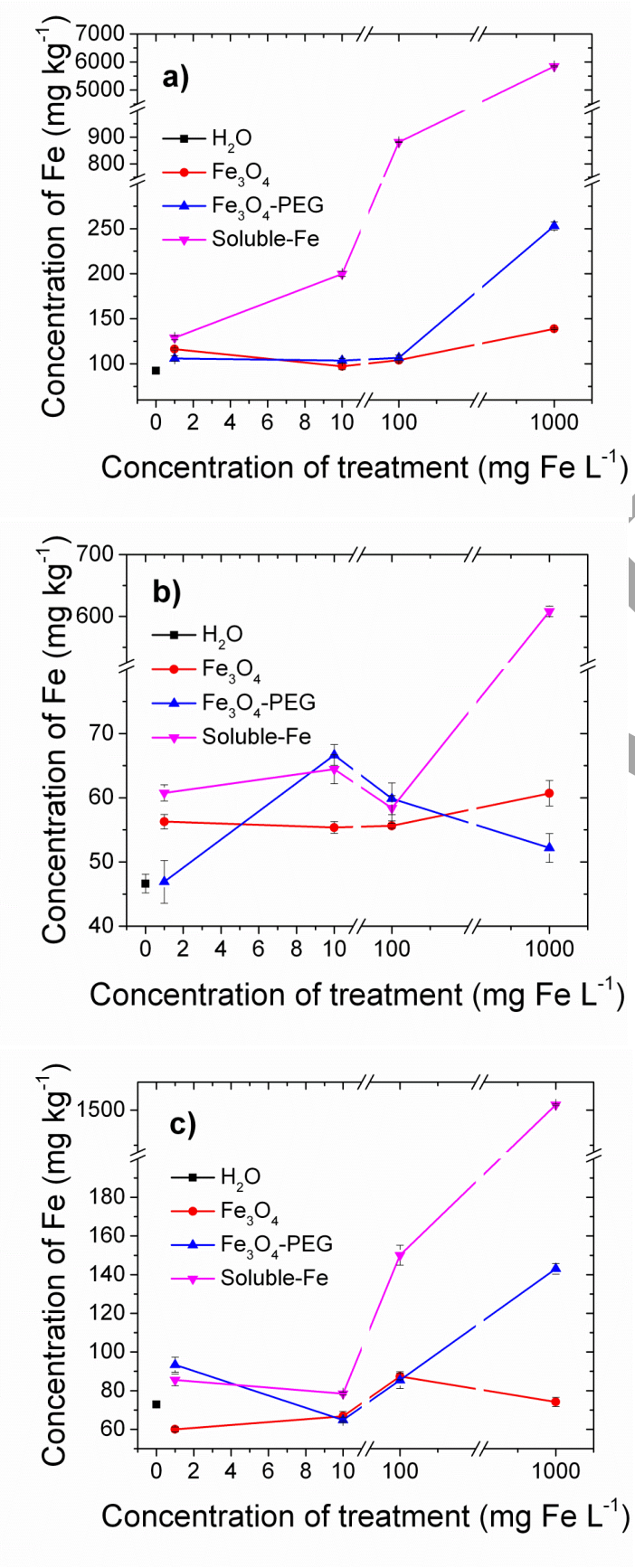

Figure 5

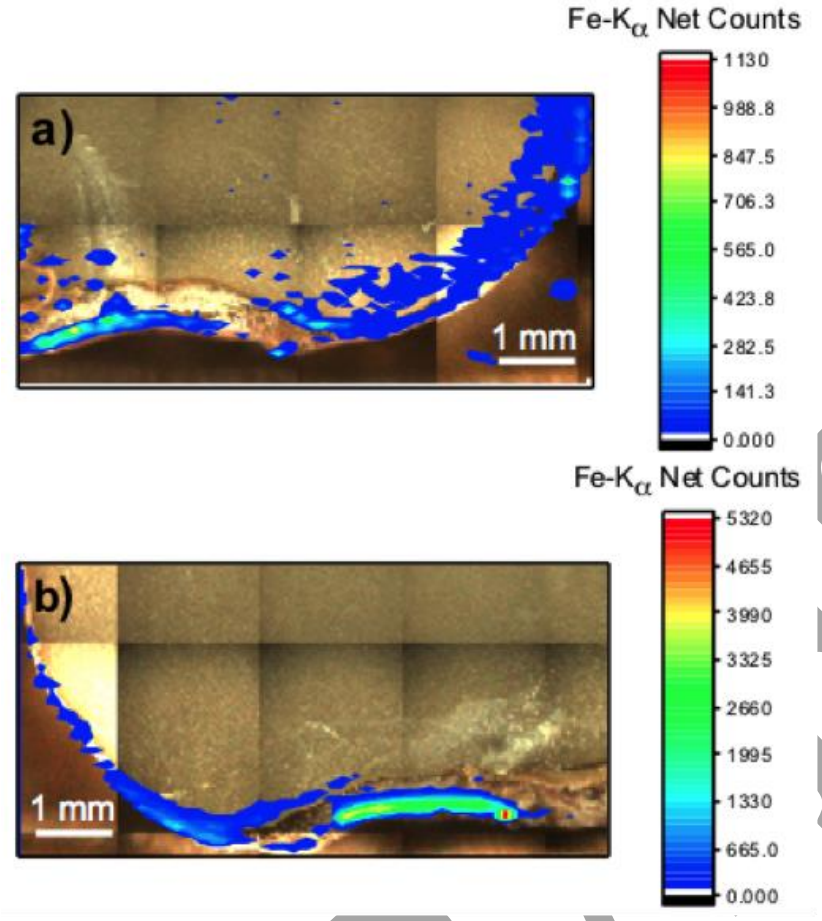

Figure 6

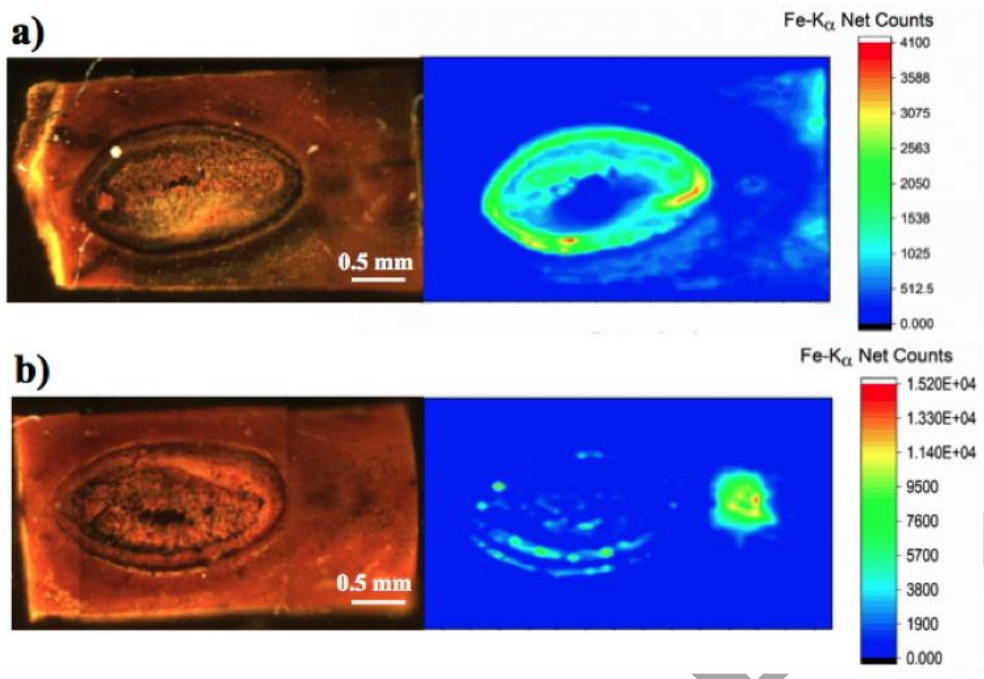

Figure 7

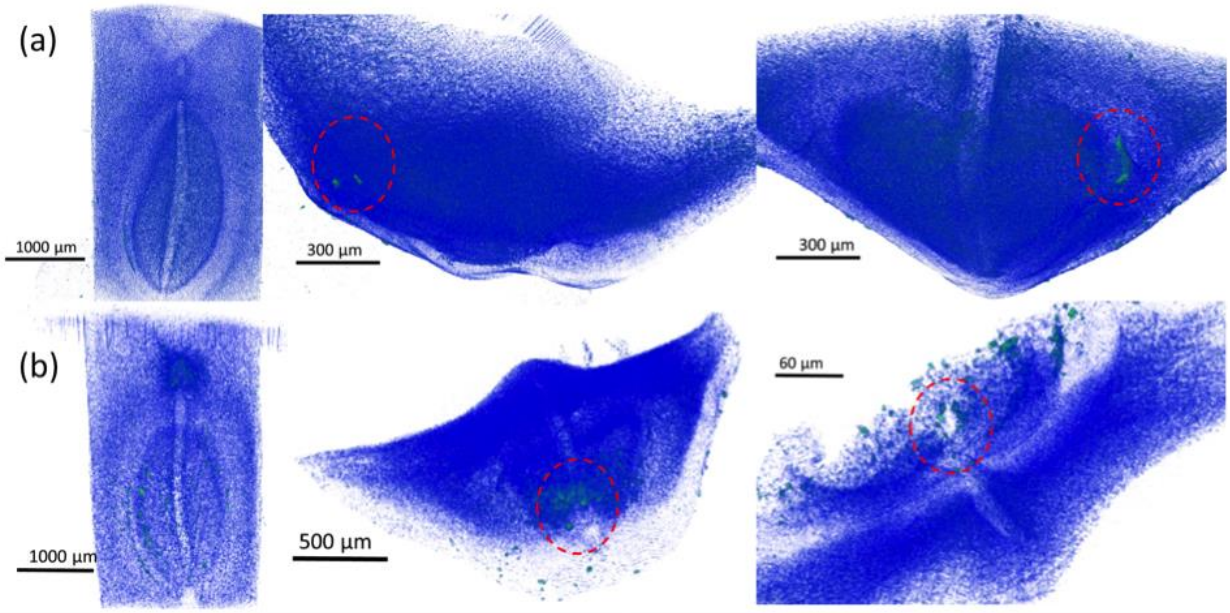

GRAPHIC FOR TABLE OF CONTENTS